




# Origin of the anomalous Pb-Br bond dynamics in formamidinium lead bromide perovskites

Harishchandra Singh,<sup>1</sup> Ruixiang Fei,<sup>2</sup> Yevgeny Rakita<sup>3</sup>,,<sup>3</sup> Michael Kulbak<sup>3</sup>,,<sup>3</sup> David Cahen,<sup>3</sup>  
Andrew M. Rappe,<sup>2,\*</sup> and Anatoly I. Frenkel<sup>1,†</sup>

<sup>1</sup>Department of Materials Science and Chemical Engineering, Stony Brook University, Stony Brook, New York 11794, USA

<sup>2</sup>Department of Chemistry, University of Pennsylvania, Philadelphia, Pennsylvania 19104-6323, USA

<sup>3</sup>Department of Materials and Interfaces, Weizmann Institute of Science, Rehovot 76100, Israel



(Received 18 August 2019; accepted 27 January 2020; published 10 February 2020)

Extended x-ray absorption fine structure spectroscopy of the light-harvesting formamidinium lead bromide (FAPbBr<sub>3</sub>) perovskite, a system with attractive optoelectronic performance, shows anomalously large variance in Pb-Br bond length, some 50% larger than in its inorganic CsPbBr<sub>3</sub> counterpart. Using first-principles molecular dynamics simulations, we find a significant contribution to this variance coming from the FA cation, and show that the FA does not just tumble in its cuboctahedral Br<sub>12</sub> cage, but instead stochastically sticks to, and detaches from one of the 12 nearest Br atoms after another, leading to the large variance in Pb-Br bond length. Our results demonstrate dynamic coupling between the FA-Br moiety and perovskite cage vibrations, and that tunability in dynamics can be achieved by changing the cation type and perovskite lattice parameter. Thus, our results provide information that needs to be considered in any of the intensely debated models of electron-phonon coupling in lead halide perovskites.

DOI: [10.1103/PhysRevB.101.054302](https://doi.org/10.1103/PhysRevB.101.054302)

## I. INTRODUCTION

Owing to their unique electronic properties and contribution to outstanding power conversion efficiencies of solar cells, organic and inorganic lead-halide perovskites (e.g., FAPbX<sub>3</sub>, MAPbX<sub>3</sub> and CsPbX<sub>3</sub>, where formamidinium (FA) and methylammonium (MA) are the organic components and X is a halogen, Cl/Br/I) are the focus of intense theoretical and experimental investigations [1–6]. The sources of the observed structural disorder [7–15], and their possible correlations with optoelectronic properties in these perovskites are intensely debated [8,13,16,17]. Because it has been shown that those properties are defined by the metal-halogen interactions [13,18], understanding the detailed behavior of the Pb-X bond length disorder may well help to provide a solid basis for the relation between mechanical and optoelectronic properties of these materials. The samples selected for this study are the well-characterized organic lead-halide FAPbBr<sub>3</sub> and inorganic lead-halide CsPbBr<sub>3</sub> materials, both of which contain Pb-Br bonds. By combining extended x-ray absorption fine structure (EXAFS) spectroscopy with *ab initio* molecular dynamics simulations (MD), we align model-independent measurements of the disorder in these perovskites with atomic- and electronic-scale interpretation and analysis, highlighting the influence of the organic cations on the dynamics of the inorganic framework.

The samples were thin films, CsPbBr<sub>3</sub> (50 nm) and FAPbBr<sub>3</sub> (500 nm), spin-coated onto a glass microslide; details on fabrication can be found in the Supplemental Material [19] (see, also, Refs. [20–30] therein). EXAFS measurements

at Pb *L*<sub>3</sub> and Br *K* edges allowed us to focus on these atomic species (Pb and Br). Pb and Br form bonds along all the edges of the perovskite unit cell (Fig. 1) forming the structural framework common to the organic and inorganic perovskites. Therefore, probing these Pb-Br bonds by comparing their vibrational properties in these two systems gives a sensitive probe of structural dynamics.

EXAFS measurements at the Pb *L*<sub>3</sub> edge (13.035 keV) and Br *K* edge (13.474 keV) were collected at the 5BM DND CAT beamline at the Advanced Photon Source (APS) of the Argonne National Laboratory, where a four-channel Vortex detector has been used to collect the fluorescence data. EXAFS data were processed using conventional procedures, as described in the Supplemental Material.

## II. RESULTS AND DISCUSSION

The *k*<sup>2</sup>-weighted EXAFS data for Pb and Br edges for both samples are shown in *k* space [see the Supplemental Material, Fig. S1] and *r* space (Fig. 2). The Br *K* edge spectra have a split first shell peak in *r* space [Fig. 2(b)], due to the Ramsauer-Townsend effect in the backscattering amplitude of Pb [31]. The main effect, evident in the *k* space and *r* space data of both Br and Pb edges, is the strong decrease of the signal intensity of the FAPbBr<sub>3</sub> sample compared to that in the CsPbBr<sub>3</sub> sample. We briefly outline possible causes for these changes that we will quantitatively analyze in the subsequent section. One reason for this effect could be the decrease in the Pb-Br (and Br-Pb) coordination number in the organic sample, compared to the inorganic one. Another reason for this effect could be the relative increase of the Pb-Br bond length disorder in the organic sample. However, the change in the coordination numbers is not reasonable in three-dimensional perovskites, as the Pb environment remains

\*Corresponding author: rappe@sas.upenn.edu

†Corresponding author: anatoly.frenkel@stonybrook.edu

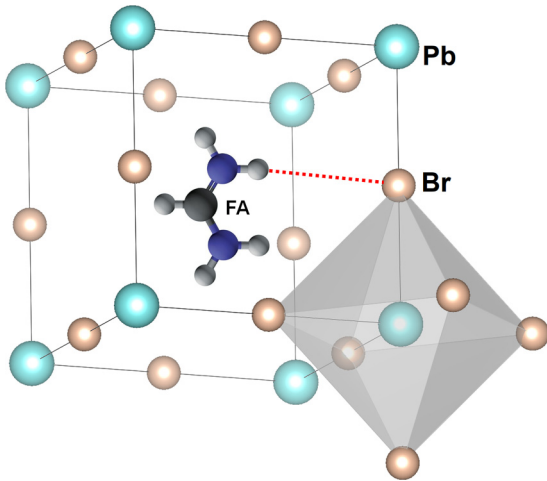


FIG. 1. Schematic of the FAPbBr<sub>3</sub> structure. Dotted line denotes the *shortest* instantaneous H-Br distance during the rotation of an FA cation.

hexadentate. An enhanced disorder in the organic sample is, thus, the most reasonable explanation for the data. We have also examined, and subsequently ruled out, the x-ray beam damage effect as a possible cause of the changes in the organic sample EXAFS spectra compared to the inorganic ones (see Supplemental Material, Figs. S2 and S3).

Because EXAFS measurement provides almost instantaneous “snapshots” of the structure (with characteristic time of each snapshot of  $\approx 1$  fs), information about bond dynamics is stored in the EXAFS spectra via the mean-squared disorder  $\sigma_{\text{dyn}}^2$ . If static (configurational) disorder  $\sigma_{\text{st}}^2$  is present as well as dynamic disorder, and it is statistically independent of  $\sigma_{\text{dyn}}^2$ , then both types of disorder will contribute to the total disorder:  $\sigma^2 = \sigma_{\text{st}}^2 + \sigma_{\text{dyn}}^2$ , which is measured by EXAFS. To understand the nature of the dramatic intensity change (Fig. 2) observed in these materials, we focused on the investigation of the dynamic behavior, by combining quantitative EXAFS analysis and MD simulations.

The resultant EXAFS signals were analyzed in  $r$  space using FEFF6 [32] and Artemis codes from the DEMETER package [33]. For the Br edge, the Br-Pb first nearest-neighbor path, and for the Pb edge, the Pb-Br paths were included in their respective fits. The details of the FEFF calculations,

fitting model and Fourier transform parameters used in the fits are summarized in the Supplemental Material. The data and fits to the Pb  $L_3$  and Br  $K$  edge spectra in both samples are shown in the Supplemental Material, Fig. S4 in  $r$  space. Consistent with the visual observation (Fig. 2), the values of the Pb-Br bond length disorder in the organic perovskite sample were obtained to be approximately 50% larger than in the inorganic one:  $\sigma_{\text{FA}}^2 = 0.0209 \pm 0.0013 \text{ \AA}^2$  vs  $\sigma_{\text{Cs}}^2 = 0.0144 \pm 0.0019 \text{ \AA}^2$ .

This difference between the disorder parameters ( $0.0065 \pm 0.0023 \text{ \AA}^2$ ) of the Pb-Br bond is comparable to that ( $0.0041 \pm 0.0007 \text{ \AA}^2$ ) reported for another bond type, Rb-Cl, which is a common bond in two types of alkali halides, RbCl and Rb(Br,Cl), a solid solution of RbBr and RbCl, that were measured by EXAFS at 30 K [34]. In those materials, the larger  $\sigma^2$  value of  $0.0096 \pm 0.0005 \text{ \AA}^2$  was found in the mixed system and its difference from the corresponding value ( $0.0055 \pm 0.0005 \text{ \AA}^2$ ) in pure RbCl was attributed to bond buckling [34], due to loss of contact of the smaller  $\text{Cl}^-$  (compared to  $\text{Br}^-$ ) anions with their Rb neighbors in the octahedral cage. In the present case, the measurement of the Pb-Br disorder parameter is not sufficient to describe the complicated structural dynamics of FAPbBr<sub>3</sub> (or CsPbBr<sub>3</sub>) and discriminate between possible models of disorder that may include rotation or, as it was recently shown, the tumbling motion of FA cation in FAPbX<sub>3</sub> cage [35]. To address this challenge, we performed first-principles MD simulations based on density functional theory (DFT) [24–29]. These calculations were performed at 300 K, using lattice parameters of the orthorhombic and cubic CsPbBr<sub>3</sub> unit cells and cubic FAPbBr<sub>3</sub> unit cell (see the Supplemental Material). To obtain the velocity autocorrelations, the time intervals were 40-ps long, with a 10-fs time step for inorganic perovskites, and 25-ps long, with 2-fs time step for organic perovskites. We verified that, at this simulation length, the velocity autocorrelation converged.

We now focus on the two possible factors that differ between the two investigated systems: (a) the cation type (Cs vs FA) and (b) the lattice parameter. The Cs-FA substitution, accompanied by the phase change from orthorhombic CsPbBr<sub>3</sub> to cubic FAPbBr<sub>3</sub>, coupled with the difference in the effective cation size (causing greater lattice parameter in FAPbBr<sub>3</sub>) could have a complex effect on the bond length disorder. To model the lattice expansion effect, we systematically calculated the changes in the phonon density of states (p-DOS)

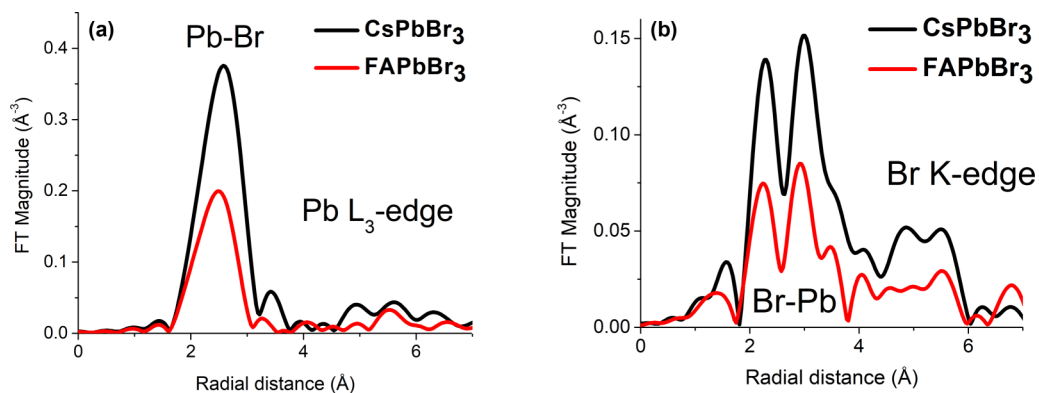


FIG. 2. Fourier transform magnitudes of the Pb  $L_3$  edge (a) and Br  $K$  edge (b)  $k^2$ -weighted EXAFS data for CsPbBr<sub>3</sub> and FAPbBr<sub>3</sub> samples.

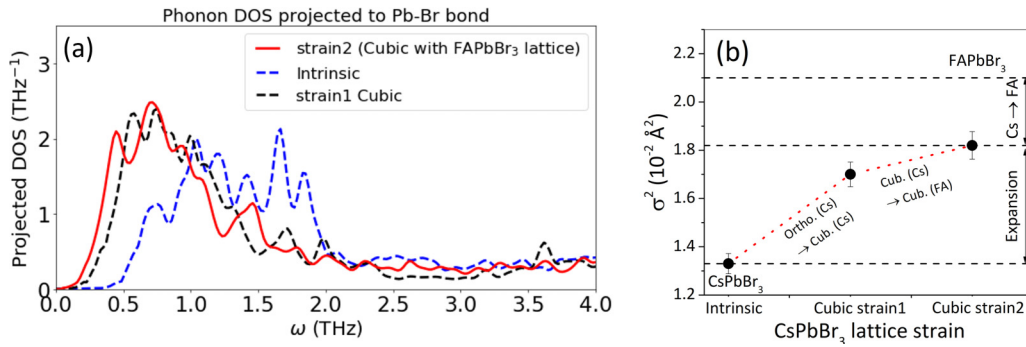


FIG. 3. The PDOS of CsPbBr<sub>3</sub> projected to the Pb-Br bonds (a), and the mean square relative displacements ( $\sigma^2$ ) of Pb-Br distances in CsPbBr<sub>3</sub> at room temperature for different lattice constants and symmetries, calculated using MD simulations (b). Simulated  $\sigma^2$  value for FAPbBr<sub>3</sub> is shown as well. This computational exploration of inorganic perovskite CsPbBr<sub>3</sub> illustrates two key aspects contributing to enhanced bond disorder in the hybrid perovskite FAPbBr<sub>3</sub>, the expansion of the lattice and the compositional substitution.

for different amounts of deformation (see also Supplemental Material, Table S1), denoted as strain 1 and strain 2. The strain 1 represents the CsPbBr<sub>3</sub>, strained from an orthorhombic ( $a = 11.659$ ,  $b = 11.735$ ,  $c = 11.594$  Å) to a cubic phase ( $a = 11.735$  Å). We find that the phonon frequencies decrease with increasing tensile strain [Fig. 3(a)], and that the Pb-Br bond length disorder increases with strain [Fig. 3(b)]. Once the p-DOS  $\rho_R(\omega)$ , the vibrational density of states, projected on the bond direction  $R$ , is obtained, the mean-square relative displacement (MSRD), also known as the EXAFS Debye-Waller factor,  $\sigma_R^2$ , is given by the Debye integral  $\sigma_R^2 = \frac{\hbar}{2\mu_R} \int_0^{\omega_{\max}} d\omega \rho_R(\omega) \frac{\coth \frac{\beta\hbar\omega}{2}}{\omega}$ , where  $\mu_R$  is the reduced mass of Pb-Br pair,  $\frac{1}{\mu_R} = \frac{1}{M_{\text{Pb}}} + \frac{1}{M_{\text{Br}}}$ , and  $\beta = 1/k_B T$  [36]. As calculated over the p-DOS, the values of the Pb-Br bond length disorder were obtained to be  $\sigma_{\text{Cs}}^2 = 0.0133 \pm 0.0004$  Å<sup>2</sup> for orthorhombic CsPbBr<sub>3</sub> and  $0.0182 \pm 0.0006$  Å<sup>2</sup> for cubic CsPbBr<sub>3</sub>, using the lattice constant of FAPbBr<sub>3</sub> at room temperature. However, the simulated disorder value for the FAPbBr<sub>3</sub> was found to be  $\sigma_{\text{FA}}^2 = 0.0210 \pm 0.0006$  Å<sup>2</sup> [Fig. 3(b)], which is significantly larger than that of cubic CsPbBr<sub>3</sub> (with the same axes ratios and lengths). In addition, the simulated and the experimental disorder values ( $0.0209 \pm 0.0013$  Å<sup>2</sup> for the cubic FAPbBr<sub>3</sub> and  $0.0144 \pm 0.0019$  Å<sup>2</sup> for the orthorhombic CsPbBr<sub>3</sub>) are in remarkable agreement. Hence, one can be confident that the enhanced disorder of cubic FAPbBr<sub>3</sub> must have a significant and direct contribution from the organic moiety [Fig. 3(b)], namely the FA makes a large contribution to the Pb-Br bond disorder in the cubic phase.

MD simulations provide insight into the origin of this enhanced dynamic disorder in the hybrid perovskite. Figure S5a illustrates the conventional bond length dynamics in cubic CsPbBr<sub>3</sub>, in which the Pb-Br and Br-Cs pairs oscillate about their average lengths calculated from the MD trajectory using eight formula unit supercells. The variation range of Pb-Br bond length is 0.3 Å in CsPbBr<sub>3</sub> (Fig. S5a), in striking contrast with the Pb-Br bond length behavior in FAPbBr<sub>3</sub> (Fig. S3b) that exhibits much larger fluctuations. Figure 4(a) reveals that large variations of the Pb-Br bond lengths correlate with the strongly nonrotational “sticky” motion of FA cation. This conclusion is deduced from the negative value (at  $\Delta t = 0$ )

of the normalized cross-correlation function of the Pb-Br and H-Br shortest distances containing the same Br atom. Figure S5b plots the time-dependence of the H-Br distances, which connect a given Br atom with the nearest H atom in a given FA cation. *This strong anticorrelation means that a particularly short H-Br bond frequently occurs at the same time when the Br-Pb bond is elongated, suggesting that the interactions of the organic cation with Br influence the Pb-Br structure backbone.* In Fig. 4(b), we compare the shortest H-Br distance calculated from the MD trajectory over the entire simulation box with that from the simple hypothetical rotational motion of the FA cation. This demonstrates that this cation displaces off-center and H bonds are formed, leading to shorter H-Br bonds than expected. The details of these calculations are given in the Supplemental Material.

We obtained larger changes for the shorter Pb-Br distance of the two bonds between any Br atom and its nearest Pb neighbors and, hence, Fig. S3b, shows only the shortest Pb-Br distance behavior. As shown in Fig. 4(b), FA spends significant time (on average, 91%) by sticking and remaining close to one of the 12 nearest Br atoms. In this respect, the FA cation is almost never located in the FABr<sub>12</sub> cuboctahedron center, corresponding to the average structure. Instead, it is locally displaced from the center of the FA mass, stochastically sticking to, and separating from one of the nearest 12 Br atoms. This model has some fascinating similarities with the order-disorder “eight site model” [37,38], in which the central Ti atoms in the high-temperature phase of BaTiO<sub>3</sub> are located at the TiO<sub>6</sub> octahedron centers only on average, while locally all Ti atoms are displaced in one of the eight (111) lattice directions.

Whereas discrete rotational reorientations of FA cation in FAPbI<sub>3</sub> perovskite were detected by MD simulations before [39], our MD simulations, combined with our experimental EXAFS results, provide evidence of the direct impact of the anomalous FA-X dynamics on the cage vibration. Results of our combined analysis fully explain the observed increase of the Pb-Br bond length disorder in the FAPbBr<sub>3</sub> compared to CsPbBr<sub>3</sub>. The good quantitative agreement between theory and experiment for the MSRD values of both orthorhombic CsPbBr<sub>3</sub> and cubic FAPbBr<sub>3</sub> allowed us to rely on the details of MD simulations to disentangle between the different possible contributions to lattice dynamics of the Pb-Br cage. Our

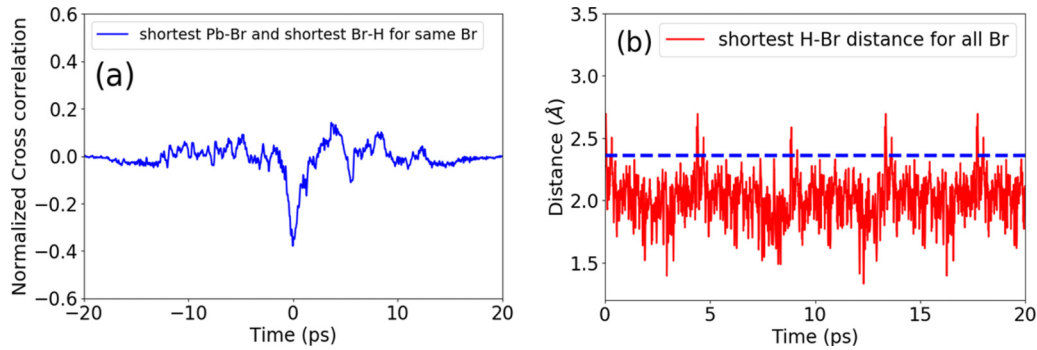


FIG. 4. (a) The normalized cross-correlation function of the shortest H-Br distances and the Pb-Br distances for the same Br atom in FAPbBr<sub>3</sub>, calculated from the MD trajectory. The negative value at  $\Delta t = 0$  indicates that the formation of the shortest Br-H bonds coincides in time with elongation of the Pb-Br bonds for the same Br atoms. (b) The shortest H-Br for the Pb<sub>8</sub> nearest-neighbor cube, calculated from the MD trajectory of FAPbBr<sub>3</sub>. The dashed line is the shortest H-Br distance calculated using a hypothetical rigid rotational motion of the FA ion around the FA center of mass that stays at the cage center.

results demonstrate that the Pb-Br disorder in both compounds is predominantly dynamic, in good agreement with both the hypothesis made above on the basis of the difference in the structures and on the conclusion, drawn from the temperature dependence of the Urbach energy of MAPbI<sub>3</sub>, i.e., that it results dominantly from dynamic disorder (originating from the cage vibration), rather than from static disorder [40]. As a result, we are able to evaluate quantitatively the effects on the bond length disorder due to the lattice parameter change between the different structures and to evaluate the specific contribution for the cation at the A site (Cs- FA substitution) on the bond dynamics. Our MD simulations show that the composition-specific effect of FA on the Pb-Br bond dynamics is responsible for  $\sim 50\%$  of the enhancement of the total disorder, whereas the remaining half is attributed to the contribution to dynamics due to the lattice expansion. A close look at the details of MD simulations reveals that FA spends most of the time sticking close to a Br atom via hydrogen bonding, causing significant perturbations in Pb-Br bond lengths during those time intervals. These results emphasize the significance of the perturbations coming from FA-X interactions for explaining the enhanced dynamic disorder of Pb-Br in FAPbBr<sub>3</sub> compared to CsPbBr<sub>3</sub>.

### III. SUMMARY

Our results, which demonstrate dynamic coupling between the Pb-X and FA-X moieties, provide information on possible energy transfer mechanisms and the related intensely debated models of electron-lattice coupling in lead halide perovskites [41,42]. One such model links large carrier lifetime in MAPbI<sub>3</sub> to dynamic motion (*rotation*) of MA molecule at the picosecond time scale [43]. Stochastic, picosecond-long, *sticking* motion of the FA molecule can be similarly important for explaining the carrier lifetime in the FAPbBr<sub>3</sub>, one of

the unresolved challenges [44]. In addition, our findings pose challenge to the polaron concept, a commonly used recent model, to explain mobility in halide perovskites [44]. Characteristic time constants for polaron formation for organic and inorganic halide perovskites range between 0.3 and 0.7 ps [45], i.e., the same time scale as the sticking time we observed in FAPbBr<sub>3</sub> system. The FA “stickiness”, which is affected strongly by the volume of the lattice, will also contribute to the anharmonicity in Pb-X vibrations, and thus directly affect charge mobility, thermal conductivity [46], and mechanical stability of FAPbX<sub>3</sub> perovskites [47].

### ACKNOWLEDGMENTS

A.I.F. acknowledges support by National Science Foundation Grant No. DMR-1911592. R.F. and A.M.R. acknowledge support from the National Science Foundation, under Grant No. DMR-1719353. Computational support was provided by the National Energy Research Scientific Computing Center of the Department of Energy. X-ray absorption spectroscopy data were collected at the DuPont-Northwestern-Dow Collaborative Access Team (DND-CAT) located at Sector 5 of the Advanced Photon Source (APS). DND-CAT is supported by Northwestern University, E.I. DuPont de Nemours & Co., and The Dow Chemical Company. This research used resources of the Advanced Photon Source, a US Department of Energy (DOE) Office of Science User Facility operated for the DOE Office of Science by Argonne National Laboratory under Contract No. DE-AC02-06CH11357. A.I.F. and A.M.R. acknowledge support by Weston Visiting Professorships during their stays at the Weizmann Institute of Science. Y.R. and D.C. thank the US-Israel Binational Science Foundation, the Ullmann family foundation, and the Weizmann Institute’s Sustainability and Energy Research Initiative for partial support.

- [1] D. B. Mitzi, *Chem. Rev.* **119**, 3033 (2019).  
 [2] A. K. Jena, A. Kulkarni, and T. Miyasaka, *Chem. Rev.* **119**, 3036 (2019).  
 [3] Q. Tai, K.-C. Tang, and F. Yan, *Energy Environ. Sci.* **12**, 2375 (2019).

- [4] H. Tsai, R. Azadpour, J.-C. Blancon, C. C. Stoumpos, O. Durand, J. W. Strzalka, B. Chen, R. Verduzco, P. M. Ajayan, S. Tretiak *et al.*, *Science* **360**, 67 (2018).  
 [5] Q. A. Akkerman, G. Rainò, M. V. Kovalenko, and L. Manna, *Nat. Mater.* **17**, 394 (2018).

- [6] J. Huang, Y. Yuan, Y. Shao, and Y. Yan, *Nat. Rev. Mater.* **2**, 17042 (2017).
- [7] S. Kanno, Y. Imamura, and M. Hada, *J. Chem. Phys.* **121**, 26188 (2017).
- [8] M. Fu, P. Tamarat, J.-B. Trebbia, M. I. Bodnarchuk, M. V. Kovalenko, J. Even, and B. Lounis, *Nat. Commun.* **9**, 3318 (2018).
- [9] A. Poglitsch and D. Weber, *J. Chem. Phys.* **87**, 6373 (1987).
- [10] A. M. A. Leguy, A. R. Goñi, J. M. Frost, J. Skelton, F. Brivio, X. Rodriguez-Martinez, O. J. Weber, A. Pallipurath, M. I. Alonso, M. Campoy-Quiles *et al.*, *Phys. Chem. Chem. Phys.* **18**, 27051 (2016).
- [11] O. Selig, A. Sadhanala, C. Muller, R. Lovrincic, Z. Chen, Y. L. A. Rezus, J. M. Frost, T. L. C. Jansen, and A. A. Bakulin, *J. Am. Chem. Soc.* **139**, 4068 (2017).
- [12] Y. S. Guo, O. Yaffe, D. W. Paley, A. N. Beecher, T. D. Hull, G. Szpak, J. S. Owen, L. E. Brus, and M. A. Pimenta, *Phys. Rev. Mater.* **1**, 042401(R) (2017).
- [13] O. Yaffe, Y. Guo, L. Z. Tan, D. A. Egger, T. Hull, C. C. Stoumpos, F. Zheng, T. F. Heinz, L. Kronik, M. G. Kanatzidis *et al.*, *Phys. Rev. Lett.* **118**, 136001 (2017).
- [14] M. Z. Mayers, L. Z. Tan, D. A. Egger, A. M. Rappe, and D. R. Reichman, *Nano Lett.* **18**, 8041 (2018).
- [15] X. Wu, L. Z. Tan, X. Shen, T. Hu, K. Miyata, M. T. Trinh, R. Li, R. Coffee, S. Liu, D. A. Egger *et al.*, *Sci. Adv.* **3**, e1602388 (2017).
- [16] F. Panzer, C. Li, T. Meier, A. Kohler, and S. Huettner, *Adv. Energy Mater.* **7**, 1700286 (2017).
- [17] S. Singh, C. Li, F. Panzer, K. L. Narasimhan, A. Graeser, T. P. Gujar, A. Kohler, M. Thelakkat, S. Huettner, and D. Kabra, *J. Phys. Chem. Lett.* **7**, 3014 (2016).
- [18] Z. Xiao and Y. Yan, *Adv. Energy Mater.* **7**, 1701136 (2017).
- [19] See Supplemental Material at <http://link.aps.org/supplemental/10.1103/PhysRevB.101.054302> for technical details on sample preparation, EXAFS data, processing and analysis results, and details on DFT and MD calculations.
- [20] Y. Rakita, N. Kedem, S. Gupta, A. Sadhanala, V. Kalchenko, M. L. Bohm, M. Kulbak, R. H. Friend, D. Cahen, and G. Hodes, *Crystal Growth Des.* **16**, 5717 (2016).
- [21] M. Kulbak, S. Gupta, N. Kedem, I. Levine, T. Bendikov, G. Hodes, and D. Cahen, *J. Phys. Chem. Lett.* **7**, 167 (2016).
- [22] M. Kulbak, D. Cahen, and G. Hodes, *J. Phys. Chem. Lett.* **6**, 2452 (2015).
- [23] M. Newville, P. Livins, Y. Yacoby, J. J. Rehr, and E. A. Stern, *Phys. Rev. B* **47**, 14126 (1993).
- [24] P. Giannozzi, S. Baroni, N. Bonini, M. Calandra, R. Car, C. Cavazzoni, D. Ceresoli, G. L. Chiarotti, M. Cococcioni, I. Dabo *et al.*, *J. Phys.: Condens. Matter* **21**, 395502 (2009).
- [25] J. P. Perdew, K. Burke, and M. Ernzerhof, *Phys. Rev. Lett.* **77**, 3865 (1996).
- [26] N. J. Ramer and A. M. Rappe, *Phys. Rev. B* **59**, 12471 (1999).
- [27] A. M. Rappe, K. M. Rabe, E. Kaxiras, and J. D. Joannopoulos, *Phys. Rev. B* **41**, 1227 (1990).
- [28] W. G. Hoover, *Phys. Rev. A* **31**, 1695 (1985).
- [29] S. Nosé, *J. Chem. Phys.* **81**, 511 (1984).
- [30] F. C. Hanusch, E. Wisenmayer, E. Mankel, A. Binek, P. Angloher, C. Fraunhofer, N. Giesbrecht, J. M. Feckl, W. Jaegermann, D. Johrendt *et al.*, *J. Phys. Chem. Lett.* **5**, 2791 (2014).
- [31] A. G. Mckale, B. W. Veal, A. P. Paulikas, S.-K. Chan, and G. S. Knapp, *Phys. Rev. B* **38**, 10919 (1988).
- [32] S. I. Zabinsky, J. J. Rehr, A. Ankudinov, R. C. Albers, and M. J. Eller, *Phys. Rev. B* **52**, 2995 (1995).
- [33] B. Ravel and M. Newville, *J. Synchrotron Radiat.* **12**, 537 (2005).
- [34] A. Frenkel, E. A. Stern, A. Voronel, M. Qian, and M. Newville, *Phys. Rev. Lett.* **71**, 3485 (1993).
- [35] D. Ghosh, P. Walsh Atkins, M. S. Islam, A. B. Walker, and C. Eames, *ACS Energy Lett.* **2**, 2424 (2017).
- [36] F. D. Vila, J. J. Rehr, H. H. Rossner, and H. J. Krappe, *Phys Rev B* **76**, 014301 (2007).
- [37] I. B. Bersuker, *Phys. Lett.* **20**, 589 (1966).
- [38] R. Comes, M. Lambert, and A. Guinier, *Solid State Commun.* **6**, 715 (1968).
- [39] V. C. A. Taylor, D. Tiwari, M. Duchi, P. M. Donaldson, I. P. Clark, D. J. Fermin, and T. A. A. Oliver, *J. Phys. Chem. Lett.* **9**, 895 (2018).
- [40] M. Ledinsky, T. Schönfeldová, J. Holovský, E. Aydin, Z. Hájková, L. Landová, N. Neyková, A. Fejfar, and S. De Wolf, *J. Phys. Chem. Lett.* **10**, 1368 (2019).
- [41] P.-A. Mante, C. C. Stoumpos, M. G. Kanatzidis, and A. Yartsev, *Nat. Commun.* **8**, 14398 (2017).
- [42] A. D. Wright, C. Verdi, R. L. Milot, G. E. Eperon, M. A. Pérez-Osorio, H. J. Snaith, F. Giustino, M. B. Johnston, and L. M. Herz, *Nat. Commun.* **7**, 11755 (2016).
- [43] J. Gong, M. Yang, X. Ma, R. D. Schaller, G. Liu, L. Kong, Y. Yang, M. C. Beard, M. Lesslie, Y. Dai *et al.*, *J. Phys. Chem. Lett.* **7**, 2879 (2016).
- [44] X.-Y. Zhu and V. Podzorov, *J. Phys. Chem. Lett.* **6**, 4758 (2015).
- [45] K. Miyata, T. L. Atallah, and X.-Y. Zhu, *Sci. Adv.* **3**, e1701469 (2017).
- [46] X. Qian, X. Gu, and R. Yang, *App. Phys. Lett.* **108**, 063902 (2016).
- [47] S. Sun, F. H. Isikgor, Z. Deng, F. Wei, G. Kieslich, P. D. Bristowe, J. Ouyang, and A. K. Cheetham, *ChemSusChem* **10**, 3740 (2017).